Subcritical Dynamo Bifurcation in the Taylor-Green Flow

Y. Ponty,[1] J.-P. Laval,[2] B. Dubrulle,[3] F. Daviaud,[3] and J.-F. Pinton[4]

[1]*Laboratoire Cassiopée, CNRS & Observatoire de la Côte d'Azur, Nice 06304, France*
[2]*Laboratoire de Mécanique de Lille, CNRS, Villeneuve d'Asq 59665, France*
[3]*Service de Physique de l'Etat Condensé, CNRS & & CEA Saclay,Gif-sur-Yvette 91191, France*
[4]*Laboratoire de Physique de l'École Normale Supérieure de Lyon, CNRS & Université de Lyon, Lyon 69364, France*

(Received 17 July 2007; published 29 November 2007)

We report direct numerical simulations of dynamo generation for flow generated using a Taylor-Green forcing. We find that the bifurcation is subcritical and show its bifurcation diagram. We connect the associated hysteretic behavior with hydrodynamics changes induced by the action of the Lorentz force. We show the geometry of the dynamo magnetic field and discuss how the dynamo transition can be induced when an external field is applied to the flow.

DOI: 10.1103/PhysRevLett.99.224501 PACS numbers: 47.65.−d, 91.25.Cw

Larmor is generally credited for suggesting that the magnetic field of the Sun (and, by extension, of planets and other celestial bodies) is due to dynamo action—i.e., self-generation from the motions of an electrically conducting fluid [1]. This principle has received much theoretical support [1] since then and has recently been validated by experimental observations [2–5]. Dynamo action results from an instability. When the magnetic Reynolds number R_M (ratio of induction to Joule's damping) exceeds a critical value R_M^c, the null magnetic field state looses its stability to a non-zero-magnetic field state. Because of the low value of the magnetic Prandtl number (ratio of kinematic viscosity to magnetic diffusivity) of the fluids, this instability develops over a turbulent (noisy) base state and the choice of an order parameter can be ambiguous [6]. However, we can assume that some concepts of stability theory apply (cf. later) and study whether the transition is supercritical or subcritical [7]. In most models and in all experiments, it is supercritical: R_M^c is a unique number, albeit flow dependant. For instance, $R_M^c \sim 14$ and $R_M^c \sim 18$ for the constrained Karlsruhe and Riga experiments, while $R_M^c \sim 32$ for the fully turbulent von Kármán sodium (VKS) dynamo [4]. On the other hand, the dynamo bifurcation could also be subcritical because the action of a growing magnetic field may reduce hydrodynamic turbulence and maintain dynamo action for lower R_M values. In fact, the transition can be globally subcritical if the basic state is unstable with respect to finite amplitude perturbations [8]. A characteristic hysteretic behavior results, and the dynamo operates in a range of lower values $R_M^g < R_M < R_M^c$. Subcriticality has been discussed in MHDα–ω dynamical systems [9,10], for numerical simulations of convective dynamos in spherical geometries [11], and recently for Keplerian shear flows [12].

In this Letter, we study the dynamo bifurcation using full MHD simulations, generated in a 3D-periodical domain, by the Taylor-Green (TG) forcing [13]. At low Reynolds numbers, this flow has several metastable hydrodynamics states [14]. At higher Reynolds numbers, it has a well defined mean flow together with intense turbulent fluctuations. Studies of the linear problem have shown that, while the dynamo threshold may run away in flows generated by random forcing [15], a dynamo is observed at all kinetic Reynolds numbers [16–18] in the Taylor-Green flow. We study here the fully nonlinear regime and report evidence of subcriticality in the bifurcation.

Using standard direct numerical simulation (DNS) procedures, we integrate pseudospectrally the MHD equations in a 2π-periodic box:

$$\frac{\partial \mathbf{v}}{\partial t} + \mathbf{v}\cdot\nabla\mathbf{v} = -\nabla\mathcal{P} + \mathbf{j}\times\mathbf{B} + \nu\nabla^2\mathbf{v} + \mathbf{F}, \quad (1)$$

$$\frac{\partial \mathbf{B}}{\partial t} + \mathbf{v}\cdot\nabla\mathbf{B} = \mathbf{B}\cdot\nabla\mathbf{v} + \eta\nabla^2\mathbf{B}, \quad (2)$$

together with $\nabla\cdot\mathbf{v} = \nabla\cdot\mathbf{B} = 0$; a constant mass density $\rho = 1$ is assumed. Here, $\mathbf{v}$ stands for the velocity field, $\mathbf{B}$ the magnetic field (in units of Alfvén velocity), $\mathbf{j} = (\nabla\times\mathbf{B})/\mu_0$ the current density, ν the kinematic viscosity, η the magnetic diffusivity, and $\mathcal{P}$ is the pressure. The forcing term $\mathbf{F}$ is given by the TG vortex

$$\mathbf{F}_{\mathrm{TG}}(k_0) = 2f(t)\begin{bmatrix} \sin(k_0x)\cos(k_0y)\cos(k_0z) \\ -\cos(k_0x)\sin(k_0y)\cos(k_0z) \\ 0 \end{bmatrix}, \quad (3)$$

implemented here at $k_0 = 1$. We shall consider two types of forcing: one in which $f(t)$ is set to a constant [$f(t) = 1.5$]; this is the constant force forcing considered in [16]. Another case corresponds to adjusting $2f(t)$ so that the (1, 1, 1) Fourier components of the velocity remains equal to the Taylor-Green vortex; this is the constant Taylor-Green vortex forcing considered in [17]. For the linear instability problem, both cases yield the same value of R_M^c [16,17]. In order to explore the nonlinear regime and study the response to finite amplitude perturbations, we note that three control parameters drive the instability: the magnetic and kinetic Reynolds numbers and the amplitude of an external magnetic field B_0 when applied. They are defined as

$$R_M = \frac{v_{\mathrm{rms}}^0\pi}{\eta} \qquad R_V = \frac{v_{\mathrm{rms}}^0\pi}{\nu} \qquad \Lambda = \frac{B_0}{v_{\mathrm{rms}}^0}. \quad (4)$$

Here, π is the size of one TG cell when $k_0 = 1$; the characteristic speed $v^0_{\rm rms}$ is computed from hydrodynamic runs in which the Navier-Stokes equation is not coupled to the induction equation, $v^0_{\rm rms} = \langle\sqrt{2E_V(t)}\rangle_t - E_V$ is net kinetic energy $E_V(t)$, and $\langle\cdot\rangle_t$ stands for averaging in time $(1/T\int^T dt)$. Likewise, in dynamo runs, the intensity of the magnetic field is estimated from the net magnetic energy $E_M(t)$, as $b = \langle\sqrt{2E_M(t)}\rangle_t$.

Previous works [17,18] have explored the response of TG flows to infinitesimal magnetic perturbations, as a function of the kinetic Reynolds number R_V. It was found that at any R_V, there exists a critical R^c_M above which perturbations grow exponentially. This is illustrated in Fig. 1 for a run at $R_V = 563$ and $R_M = 281$ above the critical value $R^c_M = 206$. The initial magnetic field perturbation—with an energy level $E_M = 10^{-17}$—first grows exponentially. At time $t \sim 300$, the magnetic field has reached sufficient amplitude so that it can react back onto the velocity field, saturate the instability, and reach a statistically stationary state, with approximate equipartition $E_M \sim E_V$. Times are given here in units of Eq. (1), for which 1 is very close to 1 eddy turnover time of the flow $(T_{\rm NL} = \pi/v^0_{\rm rms} \sim 1.17)$. This transition from infinitesimal perturbations builds the (solid) red curve in Fig. 2.

We have then quenched the system: at $t = 1000$, the magnetic diffusivity η is suddenly increased by a factor of 4, lowering R_M below R^c_M. After a short transient, both E_V and E_M decrease and reach a second statistically stationary state, with a non zero-magnetic energy—a new dynamo state, for which equipartition is reached again (Fig. 1). This behavior is evidence of global subcriticality [8]. The different levels of fluctuations in the two regimes suggest the possibility of different dynamo states, depending on the magnetic field or on the history of the system. As subcritical bifurcations are also associated with hysteresis cycles, we have repeated the quenching procedure starting from the same dynamo state A (obtained at $t = 1000$ at $R_V = 563$ in Fig. 1) for increasing values of η, i.e., for *decreasing* R_M values. The (time-averaged) magnetic and kinetic energy obtained after rearrangements are then recorded, and results summarized in Fig. 2 by the curve in the $B_0 = 0$ plane. Starting from point A, one can sustain the dynamo after quenching through points $A2$ to $A9$, until a value R^g_M substantially lower than R^c_M (at $A9$, $R_M = 70$ compared to $R_M = 211$ in $A3$).

We have investigated further the system behavior along the cycle by monitoring the spatial structure of the magnetic and kinetic energy densities, so as to detect possible changes in the flow structure. In a first regime, until point $A7$, the kinetic energy (and hence $v_{\rm rms}$, i.e., the turbulence intensity—see Table I) decreases and so does the magnetic energy—equipartition being essentially preserved. Past $A8$, changes occur: E_V starts to increase abruptly, while E_M continues to decrease, resulting in a decreasing ratio E_M/E_V—cf. later discussion and Fig. 4. Other global quantities are changing along this branch (see Table I). It corresponds to a modification in the spatial distribution of the magnetic energy. As seen in Fig. 3, the dynamo modes in $A7$ and $A8$ are different. At $A7$, the dynamo has a structure with magnetic energy "tubes" in which the field lines are concentrated along the diagonal direction (i.e., aligned with the energy structures). In $A8$, the dynamo has a

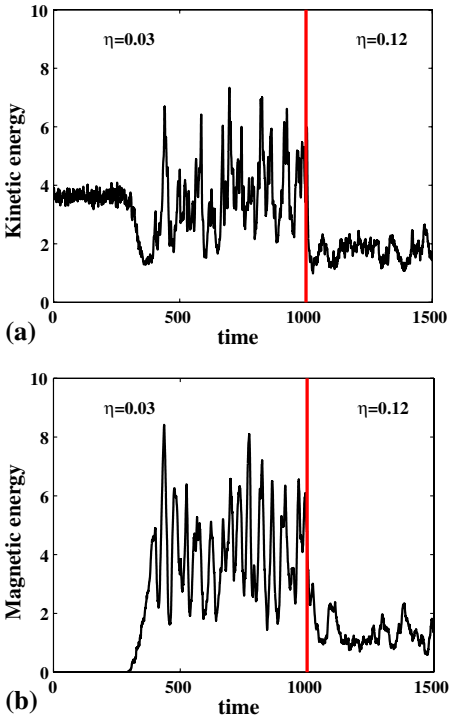

FIG. 1 (color online). After a dynamo is self-generated from infinitesimal perturbations, the induction equation is quenched at $t = 1000$ by a fourfold increase of the magnetic diffusivity. It corresponds to a sudden change from A to A_9—cf. Table I.

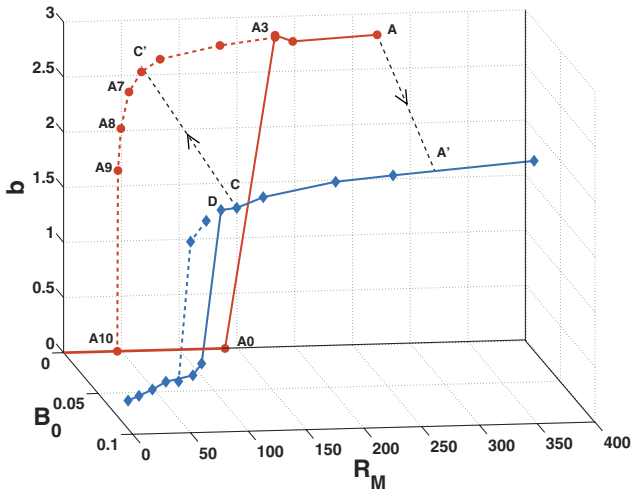

FIG. 2 (color). Bifurcation curves and hysteresis cycles when an external magnetic field is applied (full diamond symbols) or without one (full circle symbols). In this case, the subcritical quenched states (see text) form the red line. Jumps between the two branches link A to A' and C to C'.

TABLE I. The characteristics of each regime are : the root mean square amplitude of the magnetic and velocity fields $b = \langle\sqrt{2E_M(t)}\rangle_t$, $v_{\rm rms} = \langle\sqrt{2E_V(t)}\rangle_t$, the integral length scales $L_B = \langle\sum E_B(k,t)/k\rangle_t$, $L_U = \langle\sum E_V(k,t))/k\rangle_t$ computed from the one-dimensional energy spectra $E(k,t)$.

Point	η	R_M	b	L_B	$v_{\rm rms}$	L_U
A	0.03	281	2.8	5.2	2.7	3.0
$A2$	0.035	241	2.8	5.3	2.5	3.0
$A3$	0.04	211	2.8	5.4	2.5	2.9
$A4$	0.05	169	2.7	5.5	2.3	2.9
$A5$	0.07	121	2.6	5.7	2.0	2.9
$A6$	0.08	106	2.5	5.7	1.8	2.9
$A7$	0.09	94	2.4	5.7	1.7	2.9
$A8$	0.1	84	2.0	5.5	1.7	2.9
$A9$	0.12	70	1.6	5.1	1.9	3.0
$A10$	0.15	56	0.0	0.0	2.7	2.6

magnetic energy density with a wavy shape and the field lines are no longer parallel to the energy structures. In fact, the geometry of the $A8$ and $A9$ dynamo modes is reminiscent of the low kinematic mode of the TG dynamo [18].

As turbulence influences the dynamo, we have repeated the above sequence of quenching at varying kinetic Reynolds numbers R_V. The result is shown in Fig. 4. We first observe that the hysteretic behavior persists as R_V is lowered. In addition, the hysteresis cycle width, $R_M^c - R_M^g$, decreases with R_V. It is interesting to compare their locations with respect to the dynamo windows evidenced in [17,18] for the Taylor-Green forcing. As shown in Fig. 4, R_M^g values are almost independent of R_V and lie close to the beginning of the first kinematic dynamo mode. The onset R_M^c switches from the kinematic low branch to the kinematic high branch as R_V increases (and turbulence develops) [17,18]. The width of the dynamo cycle is thus linked to the evolution of the $R_M^c(R_V)$ curve. The above results were obtained with a constant force scheme. We have repeated the quenching procedure for the constant Taylor-Green vortex case. As seen in Fig. 4 (black curve/diamonds symbols), the hysteretic behavior remains, but the transition towards the nondynamo state is more abrupt. Another difference concerns the response to quenching. With a constant velocity forcing, we reach a lower magnetic saturation level; when the velocity is kept constant, there may be less possibility for the Lorentz force to change the flow.

Finally, we have checked the influence of finite amplitude external perturbations on the hysteresis cycle by applying an external magnetic field of amplitude $B_0 = 0.07$ in the vertical direction. The result at $R_V = 563$ is shown by the blue line in Fig. 2. When comparing to the $B_0 = 0$ case (red curve), two effects are readily observed: (i) the hysteresis cycle is shortened due to a decrease in the onset R_M^c from infinitesimal perturbations; (ii) the amplitude of the magnetic energy in the dynamo is decreased, as lower b values are obtained. These observations are indications that the external magnetic field has mediated a transition towards another equilibrium state [14]. The tran-

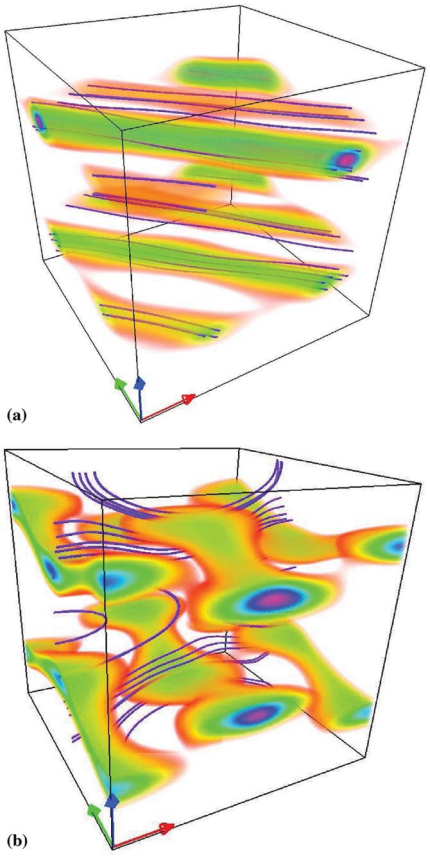

FIG. 3 (color). Volume rendering (75% of max(b)) of the magnetic energy and magnetic field lines [27], for the normalized magnetic field $\langle B(\mathbf{x},t)/B(t)\rangle$ averaged in time during the run; (a) point $A7$ and (b) point $A8$.

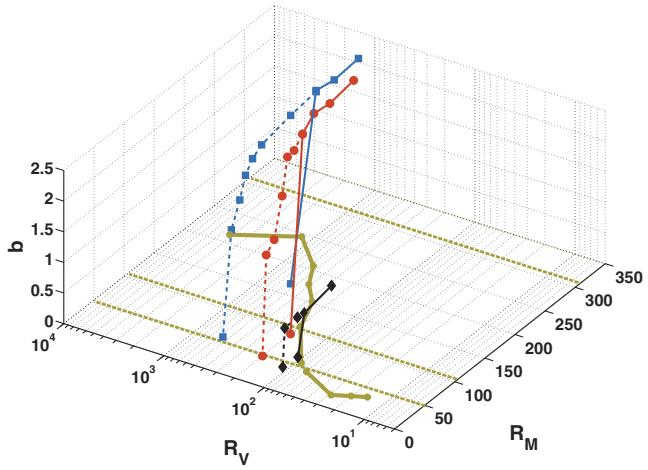

FIG. 4 (color). Hysteresis cycle for different Reynolds numbers and forcings—constant force (red, blue) and constant Tayor-Green vortex (black). The thick solid line in the $b = 0$ plane is the linear instability R_M^c vs R_V from dynamical runs; the kinematic dynamo windows [18], $R_M \in [50\ 110]$ and $R_M > 320$, are delimited by the thick dotted lines.

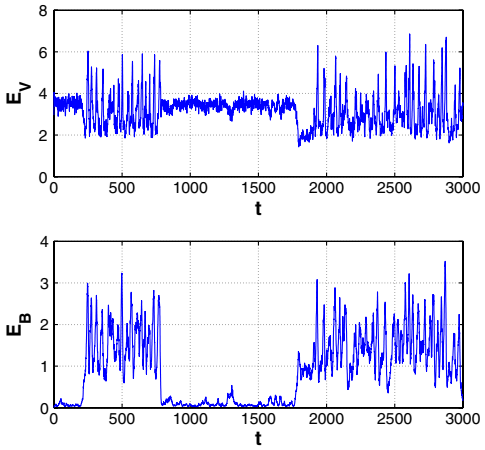

FIG. 5 (color online). Evolution on time of the kinetic (E_V) and magnetic energy (E_B) when the flow is operated in the immediate vicinity of point D—shown in Fig. 2.

sition towards this second equilibrium state is quite robust: one can also obtain it by switching on the vertical magnetic field starting from a state with a well-developed dynamo (jump from A to A' in Fig. 2). Conversely, starting from a dynamo state with an applied magnetic field and switching it off, one returns to the zero-magnetic field hysteresis curve (jump from C to C' in Fig. 2).

A less deterministic behavior is observed when the system is operated in the vicinity of point D—shown along the blue curve in Fig. 2. At this point, the system is operated at a magnetic Reynolds number slightly smaller than the linear threshold (93.8 compared to about 100) and one observes spontaneous switches between dynamo and nondynamo states, as shown in Fig. 5. This is reminiscent of the ''on-off'' bifurcation scenario sometimes proposed for the dynamo [19–22] at high R_V. It has been observed in models [23] and experimental [24] versions of the Bullard dynamo [25], and possibly in turbulent fluid dynamos [5]. We note in Fig. 5 that the kinetic energy has stronger fluctuations during the dynamo periods.

To summarize, we have evidenced in the TG flow several features characteristic of subcriticality of the dynamo instability. At variance with typical dynamical systems, this behavior is obtained in a fully turbulent system, where fluctuations are of the same order of magnitude as the mean flow. We may remark that in this case, the traditional concept of amplitude equation may be ill-defined and one may have to generalize the notion of ''subcritical transition'' for turbulent flows. Another feature is the sensitivity to perturbations of the order parameter through the application of an external magnetic field. The perturbation mainly acts through macroscopic changes in the system configuration (perturbation of the velocity field), allowing lower thresholds for dynamo instability. These findings open new perspective for experimental dynamos. For the TG flow, we observe a decrease of the dynamo threshold by as much as 57%, with an external applied field of $B_0 = 0.07$. We have also found that changes in the geometry of the dynamo states in the subcritical branch are consistent with the coexistence of several metastable hydrodynamics states [14]. Preliminary observations in the VKS experiment also point to the existence of subcritical dynamos in the presence of global rotation [26], a feature also noted in some numerical models of the geodynamo [11].

We acknowledge useful discussions with A. Pouquet and P. Mininni, R. Jover, and team members of the VKS collaboration. Computer time was provided by IDRIS and SIGAMM at Observatoire de la Côte d'Azur. This work is supported by the French GDR Dynamo. Y. P. thanks A. Miniussi for computing design assistance.

[1] H. K. Moffatt, *Magnetic Field Generation in Electrically Conducting Fluids* (Cambridge U. Press, Cambridge, England, 1978).
[2] A. Gailitis *et al.*, Phys. Rev. Lett. **86**, 3024 (2001).
[3] R. Stieglitz and U. Müller, Phys. Fluids **13**, 561 (2001).
[4] R. Monchaux *et al.*, Phys. Rev. Lett. **98**, 044502 (2007).
[5] M. Berhanu *et al.*, Europhys. Lett. **77**, 59001 (2007).
[6] VKS team (private communication); M. Berhanu *et al.*, ''Bistability between stationary and oscillating dynamos in the VKS experiment,'' report 2007 (unpublished).
[7] P. Manneville, *Dissipative Structures and Weak Turbulence* (Academic Press, Boston, 1990).
[8] O. Dauchot and P. Manneville, J. Phys. II **7**, 371 (1997).
[9] K. A. Robbins, Proc. Natl. Acad. Sci. U.S.A. **73**, 4297 (1976).
[10] S. Fedotov, I. Bashkirtseva, and L. Ryashko, Phys. Rev. E **73**, 066307 (2006).
[11] V. Morin, Ph.D. Thesis, University Paris VI , 1999; U. R. Christensen, P. Olson, and G. A. Glatzmaier, Geophys. J. Int. **138**, 393 (1999).
[12] F. Rincon, G. I. Ogilve, and M. R. E. Proctor, Phys. Rev. Lett. **98**, 254502 (2007).
[13] M. Brachet, Fluid Dyn. Res. **8**, 1 (1991); C. Nore *et al.*, Phys. Plasmas **4**, 1 (1997).
[14] B. Dubrulle *et al.*, New J. Phys. **9**, 308 (2007).
[15] A. A. Schekochihin *et al.*, New J. Phys. **4**, 84 (2002); A. A. Schekochihin *et al.*, Phys. Rev. Lett. **92**, 054502 (2004); A. B. Iskakov *et al.*, Phys. Rev. Lett. **98**, 208501 (2007).
[16] Y. Ponty *et al.*, Phys. Rev. Lett. **94**, 164502 (2005).
[17] J.-P. Laval *et al.*, Phys. Rev. Lett. **96**, 204503 (2006).
[18] Y. Ponty *et al.*, New J. Phys. **9**, 296 (2007).
[19] S. Lozhkin, D. Sokoloff, and P. Frick, Astronomy Reports **43**, 753 (1999).
[20] D. Sweet *et al.*, Phys. Rev. E **63**, 066211 (2001).
[21] N. Leprovost and B. Dubrulle, Eur. Phys. J. B **44**, 395 (2005).
[22] M. D. Nornberg *et al.*, Phys. Rev. Lett. **97**, 044503 (2006).
[23] N. Leprovost, B. Dubrulle, and F. Plunian, Magnetohydrodynamics **42**, 131 (2006).
[24] M. Bourgoin *et al.*, New J. Phys. **8**, 329 (2006).
[25] E. C. Bullard, Proc. Cambridge Philos. Soc. **51**, 744 (1955).
[26] VKS team (private communication); M. Berhanu *et al.*, Bistability between a stationary and an oscillatory dynamo in a turbulent flow of liquid sodium, report, 2007 (to be published).
[27] Imagery using VAPOR code (www.vapor.ucar.edu).